Niobium(V) Alkoxides. Synthesis, Structure, and Characterization of $[Nb(\mu\text{-}OCH_2CH_3)(OCH_2C(CH_3)_3)_4]_2$, $\{[H_3CC(CH_2O)(CH_2\text{-}\mu\text{-}O)(C(O)_2)]Nb_2(\mu\text{-}O)(OCH_2CH_3)_5\}_2$, and $\{[H_3CC(CH_2O)_2(CH_2\text{-}\mu\text{-}O)]Nb(OCH_2CH_3)_2\}_2$ for Production of Mixed Metal Oxide Thin Films[1]

Timothy J. Boyle,*,† Todd M. Alam,‡ Duane Dimos,‡ Gregorio J. Moore,† Catherine D. Buchheit,† Husam N. Al-Shareef,†,§ Eric R. Mechenbier,† and Blakely R. Bear†

Sandia National Laboratories, Advanced Materials Laboratory, MS 1349, 1001 University Boulevard SE, Albuquerque, New Mexico 87106, and Sandia National Laboratories, MS 1407, P.O. Box 5800, Albuquerque, New Mexico 87185

Joseph W. Ziller

Department of Chemistry, X-ray Diffraction Laboratory, University of California—Irvine, Irvine, California 92717

Received July 15, 1997. Revised Manuscript Received September 9, 1997[⊗]

We have synthesized and isolated a number of unique niobium alkoxide compounds and introduced them into novel solution processes for the production of lead magnesium niobate oxide (PMN) and niobium-doped lead zirconate titanate oxide (PNZT) materials. A more sterically demanding analogue to $Nb(OEt)_5$ (Et = CH_2CH_3) was isolated as $[Nb(\mu\text{-}OEt)(ONp)_4]_2$ (**1**, Np = $CH_2C(CH_3)_3$) by alcoholysis exchange. **1** crystallized in an edge-shared bioctahedral dinuclear arrangement with the smaller ligands acting as the bridging moieties. Multidentate ligands such as bis(hydroxymethyl)propionic acid (BHMP−H_3) and tris(hydroxymethyl)ethane (THME−H_3) were independently reacted with $Nb(OEt)_5$ to reduce the number of terminal ligands, yielding $[(\mu\text{-BHMP})Nb_2(\mu\text{-O})(OEt)_5]_2$ (**2**) and $[(\mu\text{-THME})Nb(OEt)_2]_2$ (**3**) respectively. For **2**, two unsymmetrical "$(EtO)_2Nb(\mu\text{-O})Nb(OEt)_3$" units are bridged by two tetradentate BHMP ligands. The THME moiety of **3** acts as a chelating, unidentate-bridging ligand forming a symmetrical dinuclear species, wherein each Nb atom possesses two terminal ethoxides. The synthesis, characterization, structural aspects, and solution properties of **1**−**3** are reported. The resulting morphological and electrical changes in the properties of the resulting electroceramic PMN and PNZT films due to the incorporation of these Nb alkoxides are also reported.

Introduction

Due to their electrical and electromechanical properties, thin films of both ferroelectric and relaxor ferroelectric materials are of great interest for a wide range of applications from nonvolatile random access memories (NVRAMs), to microelectrical mechanical devices, to integratable capacitors. Ferroelectric materials are those that possess a spontaneous polarization that can be reoriented with an applied electric field.[2] This leads to hysteresis in the polarization-voltage response and is the basis for NVRAM applications. The most widely studied class of ferroelectric thin films is based on the perovskite crystal structure of the lead zirconate titanate [$Pb(Zr_{1-x},Ti_x)O_3$; PZT] family. Aliovalent cations[3] are typically substituted for the *A*-site (Pb) and *B*-site (Zr,Ti) cations to modify the solid-state point defect chemistry and, thus, the electrical properties of the material. Niobium, which is a *B*-site donor dopant[2] (Nb^{5+} substitutes for Ti^{4+}, Zr^{4+}), is typically used to reduce the coercive (switching) voltage and improve the insulation resistance of PZT thin films.[4−7] Consequently, several research efforts are underway to understand and control formation of these PNZT [$Pb(Nb,Zr,Ti)O_3$] materials.[4−7]

Relaxor ferroelectrics, typified by the perovskite phase of lead magnesium niobate, $Pb(Mg_{1/3}Nb_{2/3})O_3$ (PMN), can be distinguished from standard ferroelectric materials based on a characteristic low-frequency dispersion

* To whom correspondences should be addressed.
† Sandia National Laboratories, Advanced Materials Laboratory, MS 1349.
‡ Sandia National Laboratories, MS 1407.
§ Current address: Micron, Technology, Inc. 800 S. Federal Way, P.O. Box 6, Boise, Idaho 83707
⊗ Abstract published in *Advance ACS Abstracts,* November 1, 1997.
(1) Portions previously presented: (a) Am. Ceram. Soc. Meeting, Jan 1995, Cocoa Beach, FL. (b) Am. Chem. Soc. Rocky Mountain Region Meeting,[2] June 1996, Denver, CO. (c) Joint Am. Ceram. Soc. and Mater. Res. Soc. Local Meeting, October 1996, Albuquerque, NM.
(2) Jaffe, B.; Cook, W. R. J.; Jaffe, H. *Piezoelectric Ceramics*; Academic Press Inc.: New York, 1971.
(3) Aliovalent indicates a dopant that has a different valence than the ion it was replacing, either higher or lower.
(4) Lee, W. I.; Lee, J. K. *Mater. Res. Bull.* **1995**, *30*, 1185.
(5) Tuttle, B. A.; Al-Shareef, H. N.; Warren, W. L.; Raymond, M. V.; Headley, T. J.; Voigt, J. A. *Microelectron. Eng.* **1995**, *29*, 223.
(6) Al-Shareef, H. N.; Tuttle, B. A.; Warren, W. L.; Dimos, D.; Raymond, M. W.; Rodriguez, M. A. *Appl. Phys. Lett.* **1996**, *68*, 272.
(7) Bjormander, C.; Sreenivas, K.; Duan, M.; Grishin, A. M.; Rao, K. V. *Microelectron. Eng.* **1995**, *29*, 111.

S0897-4756(97)00506-1 CCC: $14.00

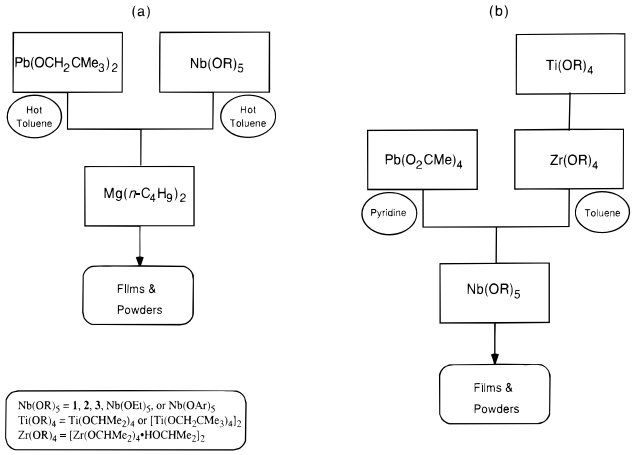

Figure 1. Schematic for synthesis of precursor solutions for (a) PMN and (b) PNZT.

of the dielectric constant[2,8,9] which is also accompanied by a broad Curie point transition. This dispersion is attributed to a disorder in the cation lattice distribution, which leads to chemically inhomogeneous microregions.[9,10] PMN relaxors are particularly interesting due to their very high permittivities and exceptional electrostrictive properties; however, the very high permittivities ($\epsilon \sim 10\,000$) attained in bulk PMN ceramics have not been achieved with PMN thin films ($\epsilon \sim 2000$).[11,12]

Solution routes are widely used for the production of thin films through spin-cast or dip-coating methodologies. These methods are typically used due to the flexibility in the stoichiometry of precursor solutions, the ease of altering processing variables, cost-effectiveness (inexpensive), the reduction of the sintering temperatures, and the integratability with existing semiconductor processes.[13−15] Figure 1 shows the schematic routes we have developed to produce the ferroelectric materials PMN[16,17] and PXZT (X = donor or acceptor dopants).[18,19] Typically soluble well-characterized precursors of high purity are desired for use in solution processes and therefore $Nb(OEt)_5$ is the primary Nb dopant precursor used. Due to the limited number of acceptable commercially available starting materials for these (and other) systems, we initiated optimization of our PMN and PNZT materials by synthesizing, characterizing, and implementing a number of novel Nb alkoxide compounds: $[Nb(\mu\text{-}OEt)(ONp)_4]_2$ (**1**), $[(\mu\text{-}BHMP)Nb_2(\mu\text{-}O)(OEt)_5]_2$ (**2**), and $[(\mu\text{-}THME)Nb(OEt)_2]_2$ (**3**) [ONp = *neo*-pentoxide; THME = tris(hydroxymethyl)-ethane; BHMP = bis(hydroxymethyl)propionic acid[21]

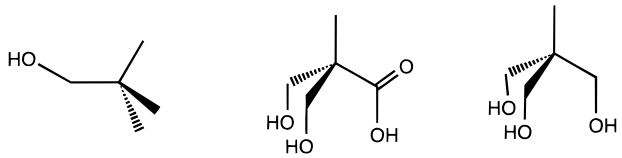

(a) (b) (c)

Figure 2. Schematic representation of ligands used for alcoholysis exchange (a) neopentanol (HONp), (b) bis(hydroxymethyl)propionic acid (BHMP−H_3), and (c) tris(hydroxymethyl)ethane (THME−H_3).

(parent alcohols are shown in Figure 2)]. This paper reports the characterization of these species in the solid state, their behavior in solution (including ^{93}Nb NMR), and the effects that these species have on the final film properties.

Experimental Section

All reactions were performed under dry nitrogen or argon, using standard Schlenk, vacuum line, and glovebox techniques. Solvents were dried, analytical data obtained, and films produced as previously described.[20] The following compounds were used as received (Aldrich): $PbCl_2$, $Mg(n\text{-}Bu)_2$ 1.0 M in heptanes, $Nb(OEt)_5$, THME−H_3, BHMP−H_3, and HONp (see Figure 2). NaONp (purified by sublimation) was isolated from a reaction between Na metal and HONp in toluene. $Pb(ONp)_2$ was synthesized with slight variations of literature procedures[22] or by the metathesis of $PbCl_2$ and NaONp.

NMR Spectroscopy. All solution ^{93}Nb NMR experiments were performed on an AMX 400 spectrometer at a resonant frequency of 97.9 MHz. The ^{93}Nb chemical shifts were referenced to external $NbCl_5$ in CH_3CN ($\delta = 0.0$), produced from doubly sublimed $NbCl_5$ and ultrapure acetonitrile.[23,24] It should be noted that care must be taken to maintain rigorously anhydrous conditions to prevent the production of the $NbCl_6^-$ ($\delta = 54$; also produced in the presence of excess halide ion[25]) or the $NbOCl_3$ ($\delta = -450$) species. Variable-temperature NMR spectra were obtained using a precalibrated thermocouple with a ±0.2 K accuracy. The temperatures that were used are noted for each compound. A 12-bit digitizer, a SW = 5000 ppm, and a standard single-pulse experiment were used to obtain spectra. All ^{1}H and ^{13}C NMR spectra were collected on either an AMX 400 at resonant frequency of 400.1 and 100.6 MHz for ^{1}H and ^{13}C, respectively, or a Bruker AC-250 at an ^{1}H resonant frequency of 250.1 MHz, with chemical shifts referenced to internal toluene-d_8.

Film Synthesis. Multilayered films of the desired composition were spin-coat deposited via a syringe (1 μm filter), in air, onto Pt-coated SiO_2/Si substrates using a photoresist spinner (3000 rpm for 30 s). After each deposition, the films were baked on a hot plate (300 °C) and allowed to cool to room temperature before introduction of the next layer. Three (~3000 Å) and 5 (~5000 Å) layer films were produced for PMN and PNZT, respectively. Films were crystallized at 700 °C for 30 min in air using a 20 °C/min ramp rate. All films were characterized by grazing incidence X-ray diffraction studies (GIXRD). Top platinum electrodes (150 μm in diameter) were deposited using a shadow mask to create a parallel-plate capacitor geometry (Pt||ferroelectric||Pt). The ferroelectric properties of the films were measured using an RT66A

(8) Cross, L. E. *Ferroelectrics* **1987**, *76*, 241.
(9) Kim, Y. S.; Jang, H. M. *Am. Ceram. Soc. Symp. Proc.* **1994**, *43*, 123.
(10) Yan, M. F.; Ling, H. C.; Rhodes, W. W. *J. Mater. Res.* **1989**, *4*, 930.
(11) Francis, L. F.; Payne, D. A. *J. Mater. Sci.* **1990**, *25*, 5007.
(12) Cross, J. S.; Tsukada, M.; Kurihara, K.; Kamehara, N.; Niwa, K. *Mater. Res. Soc. Symp. Proc.* **1995**, *361*, 483.
(13) Ramamurthi, S. D.; Payne, D. A. *J. Am. Ceram. Soc.* **1990**, *73*, 2547.
(14) Ravindranathan, P.; Komarneni, S.; Bhalla, A. S.; Cross, L. E.; Roy, R. *Mater. Res. Soc. Symp. Proc.* **1990**, *12*, 29.
(15) Vest, R. W.; Zhu, W. *Ferroelectrics* **1991**, *119*, 61.
(16) A patent application (Sandia reference number SD-5705) has been filed on this technique.
(17) Boyle, T. J.; Dimos, D. B.; Moore, G. J. *J. Am. Ceram. Soc. Symp. Proc.* **1995**, *44*, 361.
(18) Boyle, T. J.; Al-Shareef, H. N. *J. Mater. Sci.* **1997**, *32*, 2263.
(19) A patent application (Sandia reference number SD-5802) has been filed on this technique.
(20) Boyle, T. J.; Schwartz, R. W.; Doedens, R. J.; Ziller, J. W. *Inorg. Chem.* **1995**, *34*, 1110.
(21) Muller, G.; Lachmann, J.; Wunderle, J. *Z. Naturforsch.* **1993**, *43b*, 223.
(22) Goel, S. C.; Chiang, M. Y.; Buhro, W. E. *Inorg. Chem.* **1990**, *29*, 4640.
(23) Bechthold, H.-C.; Rehder, D. *J. Organomet. Chem.* **1981**, *206*, 305.
(24) Granger, P. *NMR of Newly Accessible Nuclei: Chemically and Biologically Important Elements*; Academic Press: New York, 1983; Vol. 2, Chapter 15, pp 395−396.
(25) Kidd, R. G.; Spinney, H. G. *J. Am. Chem. Soc.* **1981**, *103*, 5759.

Table 1. Data Collection for [Nb(μ-OEt)(ONp)$_4$]$_2$ (1), [(μ-BHMP)Nb$_2$(μ-O)(OEt)$_5$]$_2$ (2), and [(μ-THME)Nb(OEt)$_2$]$_2$ (3)

compound	1	2	3
chemical formula	$C_{44}H_{98}O_{10}Nb_2$	$C_{30}H_{66}O_{20}Nb_4$	$C_{18}H_{38}O_{10}Nb_2$
formula weight	973.04	1118.47	600.30
temp (K)	296	163	163
space group	$P\bar{1}$	$C2/c$	$P2_1/n$
	triclinic	monoclinic	monoclinic
a (Å)	10.424 (2)	12.284 (2)	8.479 (1)
b (Å)	10.596 (1)	20.918 (2)	9.717 (1)
c (Å)	14.528 (3)	17.913 (2)	14.583 (2)
α (deg)	111.35 (2)		
β (deg)	102.92 (4)	108.76 (1)	102.81 (1)
γ (deg)	98.01 (3)		
V (Å^3)	1413.0 (4)	4358.4 (10)	1171.5 (3)
Z	1	4	2
λ (Mo Kα radiation) (Å)	0.71073	0.71073	0.71073
D_{calcd} (Mg/m^3)	1.143	1.705	1.702
μ (Mo, Kα) (mm^{-1})	0.450	1.097	1.027
$R1$[a] (%)	9.89	3.77	3.86
$wR2$[b] [$I > 2\sigma(I)$] (%)	26.65[c]	9.36[d]	10.78[e]
$R1$[a] (%)	11.27	4.50	4.36
$wR2$[b] (all data)	28.81[c]	9.88[d]	11.30[e]

[a] $R1 = \sum||F_o| - |F_c||/\sum|F_o| \times 100$. [b] $wR2 = [\sum w(F_o^2 - F_c^2)^2/\sum(w|F_o|^2)^2]^{1/2} \times 100$. Final weighting scheme calc: [c] $w = 1/[\alpha^2(F_o^2) + (0.2069P)^2 + 5.6094P]$, [d] $w = 1/[\alpha^2(F_o^2) + (0.0510P)^2 + 42.0829P]$, [e] $w = 1/[\alpha^2(F_o^2) + (0.0864P)^2 + 0.6791P]$, where $P = (F_o^2 + 2F_c^2)/3$.

ferroelectric tester from Radiant Technologies. The dielectric properties were measured using an HP 4194A impedance analyzer.

[Nb(μ-OCH$_2$CH$_3$)(OCH$_2$CMe$_3$)$_4$]$_2$ (1). In a 250 mL pear-shaped Schlenk flask, $HOCH_2CMe_3$ (7.62 g, 86.5 mmol) was added to a stirring solution of $Nb(OEt)_5$ (5.00 g, 15.7 mmol) in toluene (100 mL). This mixture was then heated in an oil bath for 12 h at 60 °C. The solvent was removed in vacuo yielding an off-white powder, from which **1** was extracted with toluene. If necessary, this off-white powder can be used without further purification. X-ray quality crystals were grown by slow cooling of a hot toluene solution. Crystalline yield 3.44 g (45%). ^{1}H NMR (400.1 MHz, toluene-d_8) δ 4.64 (1.35 H, mult), 4.42, 4.41 (10 H, mult), 1.46 (5.4 H, mult), 1.34 (3.6 H, br s), 1.11 (36 H, s), 0.91 (6.75 H, s). ^{13}C{^{1}H}NMR (100.6 MHz, toluene-d_8) δ 84.6 (O*C*H$_2$Me, O*C*H$_2$CMe$_3$), 34.8 (OCH$_2$*C*Me$_3$), 27.5 (OCH$_2$C-*Me*$_3$), 26.9 (OCH$_2$*Me*). ^{93}Nb (97.9 MHz, 298 K, toluene-d_8) δ −1021, −1108. FT-IR (KBr pellet) 2954 (s), 2902 (m), 2868 (m), 2693 (w), 1480 (m), 1465 (m), 1442 (w), 1390 (m), 1371 (w), 1360 (m), 1292 (w), 1258 (w), 1076 (br s), 1026 (s), 935 (w), 918 (w), 905 (w), 883 (m), 848 (w), 803 (w), 751 (w), 658 (s), 560 (br s), 569 (m), 509 (m), 482 (m) cm^{-1}. TGA/DTA (oxygen; weight loss up to °C(% total weight loss)/thermal event,°C): 159 °C (1.9%)/sm endo (138 °C), 260 °C (36.3%)/sm exo (225 °C), 368 °C(53.5%)/lg exo (297 °C), 600 °C (55.2%)/sm exo (581 °C). Anal. Calcd for $C_{44}H_{98}O_{10}Nb_2$: C, 32.9; H, 6.00. Found: C, 32.3; H, 5.8.

{[H$_3$CC(CH$_2$O)(CH$_2$-μ-O)(C(O)$_2$)]Nb$_2$(μ-O)(OCH$_2$CH$_3$)$_5$}$_2$ (2). In a 250 mL Schlenk flask $H_3CC(CH_2OH)_2(C(O)OH)$ (1.30 g, 9.4 mmol) was added to $Nb(OEt)_5$ (6.00 g, 18.9 mmol) in 125 mL of toluene. The reaction mixture was heated to a boil, producing a clear solution. This mixture was allowed to cool to glovebox temperature, stirred overnight, and allowed to sit for an extended period of time. The crystals that grew at glovebox temperature proved to be {[H$_3$CC(CH$_2$-μ-O)-(CH$_2$O)(C(O)$_2$)]Nb$_2$(μ-O)(OCH$_2$CH$_3$)$_5$}$_2$ (**2**). Crystalline yield 5.70 g (54.1%). Removal of solvent after the 12 h of stirring yields an off-white powder that has analytical data consistent with the single crystals. ^{1}H NMR (250.1 MHz, toluene-d_8) δ 4.91 [1.0 H, d, J_{H-H} = 5.0 Hz, C*H*$_2$(BHMP)], 4.57 [0.8 H, d, J_{H-H} = 6.0 Hz C*H*$_2$(BHMP)], 4.30, 4.16, 4.05 [9.8 H, br s, OC*H*$_2$-CH$_3$], 3.92 [0.5 H, d, J_{H-H} = 4.0 Hz, C*H*$_2$(BHMP)], 3.71 [0.7 H, d, J_{H-H} = 5.4 Hz, C*H*$_2$(BHMP)], 1.07, 0.98 [15 H, br s, OCH$_2$C*H*$_3$], 0.63 [3.9 H, s, C*H*$_3$(BHMP)]. ^{13}C{^{1}H} (100.6 MHz, toluene-d_8) δ 75.6, 74.9, 72.5, 71.6, 70.4, 69.6, 68.8, 68.0 [O*C*H$_2$-Me, *C*H$_2$O(BHMP) and *C*O$_2$(BHMP)], 51.1 [*C* quaternary-(BHMP)], 20.0, 19.7, 19.4, 19.3, 18.8 (OCH$_2$*Me*) 14.7 [*C*H$_3$-(BHMP)]. ^{93}Nb (97.9 MHz, 298 K, toluene-d_8) δ −1135, −1185. FT-IR (KBr pellet) 2974 (m), 2930 (m), 2869 (m), 2742 (w), 2719 (w), 2701 (w), 1561 (s), 1476 (m), 1455 (w), 1427 (m), 1380 (m), 1655 (w), 1304 (m), 1279 (w), 1188 (w), 1152 (m), 1106 (s), 1064 (s), 1015 (w), 921 (s), 844 (w), 805 (w), 684 (s), 649 (m), 618 (m), 605 (m), 574 (m), 543 (m), 463 (m), 417 (m) cm^{-1}. TGA/DTA (oxygen) [weight loss up to °C (% total weight loss)/thermal event, °C]: 180 °C (1.2%)/sm endo (134 °C), 344 °C (45.6%)/lg exo (296 °C), 555 °C (51.2%)/lg exo (518 °C), 617 °C (55.2%)/lg exo (586 °C). Anal. Calcd for $C_{30}H_{66}O_{20}Nb_4$: C, 32.2; H, 5.95. Found: C, 32.3; H, 5.8.

{[H$_3$CC(CH$_2$O)$_2$(CH$_2$-μ-O)]Nb(OCH$_2$CH$_3$)$_2$}$_2$ (3). In a Schlenk flask $H_3CC(CH_2OH)_3$ (1.89 g, 15.7 mmol) was added to $Nb(OEt)_5$ (5.00 g, 15.7 mmol) in 70 mL of toluene. After stirring the reaction mixture for 12 h, the volatile fraction was removed by rotary evaporation yielding an off-white powder that was washed with hexanes (3 times). Following a toluene extraction, a white powder was isolated that had analytical data consistent with the crystalline material. X-ray quality crystals, which proved to be {[H$_3$CC(CH$_2$O)$_2$(CH$_2$-μ-O)]Nb(OCH$_2$-CH$_3$)$_2$}$_2$ (**3**), were grown by dissolving the extracted powder in a minimum of toluene and cooling the solution to −35 °C. Crystalline yield 3.40 g (72%). ^{1}H NMR (250.1 MHz, toluene-d_8) δ 4.54 (4.6 H, q, J_{H-H} = 7.0 Hz, OC*H*$_2$Me), 4.38 (1.82 H, s, C*H*$_2$(THMP)), 4.23 (4.3 H, mult, OC*H*$_2$(THME)), 1.24 (7.9 H, t, J_{H-H} = 7.0 Hz, OCH$_2$*Me*), 0.33 (3.0 H, s, *Me*(THME)). ^{13}C-{^{1}H} (62.4 MHz, APT [+, even; − odd], toluene-d_8) δ 83.7 (+, *C*H$_2$(THME)), 82.7 (+, *C*H$_2$(THME)), 74.1 (+, O*C*H$_2$Me), 48.3 (+, quaternary *C*(THME)), 23.0 (−, OCH$_2$*Me*), 19.7 (−, *Me*(THME)). ^{93}Nb (97.9 MHz, 298 K, toluene-d_8) δ −1119, −1167, −1205. FT-IR (KBr pellet) 2973 (s), 2930 (s), 2882 (s), 2850 (s), 2845 (s), 2790 (w), 2765 (w), 2670 (w), 1555 (m), 1458 (m), 1399 (m), 1375 (m), 1147 (s), 1103 (s), 1065 (s), 1021 (s), 1000 (m) 989 (s), 921 (s), 620 (s), 535 (s) cm^{-1}. TGA/DTA (oxygen) [weight loss up to °C (% total weight loss)/thermal event,°C]: 151 °C (1.3%)/sm endo(144 °C), 369 °C (28.8%)/lg exo (294 °C), 525 °C (40.7%)/lg exo (471 °C), 584 °C (42.0%)/sm exo (574 °C). Anal. Calcd for $C_{18}H_{38}O_{10}Nb_2$: C, 36.0; H, 6.38. Found: C, 36.0; H, 6.36.

X-ray Collection, Structure Determination, and Refinement. Table 1 lists the data collection parameters for **1**−**3**. Compound **1** was mounted in a glass capillary tube, whereas **2** and **3** were handled under oil before mounting on a Siemens P4 diffractometer. For all of the crystals, the determination of the Laue symmetry, crystal class, unit-cell parameters, and the orientation matrix were carried out according to standard procedures.[26] Intensity data were collected using a $2\theta/\omega$ scan technique with Mo Kα radiation. The raw data were processed with a local version of CARESS[27] that employs a modified version of the Lehman−Larsen

(26) XSCANS Software Users Guide, Version 2.1, Siemens Industrial Automation, Inc.; Madison WI 1994. XSCANS and SHELXTL PC are products of Siemens Analytical X-ray Instruments, Inc., 6300 Enterprise Lane, Madison, WI 53719

algorithm to obtain intensities and standard deviations from the measured 96-step profiles. All data were corrected for Lorentz and polarization effects and were placed on an approximately absolute scale.

For **1**, there were no systematic absences nor any diffraction symmetry other than the Friedel condition. The centrosymmetric triclinic space group $P\bar{1}$ was assigned and later determined to be correct. For **2**, the diffraction symmetry was $2/m$ with systematic absences hkl for $h + k = 2n + 1$ and $h0l$ for $l = 2n + 1$. The two possible monoclinic space groups are Cc and $C2/c$. It was later determined that the centrosymmetric space group $C2/c$ was correct. For **3**, the diffraction symmetry was $2/m$ with systematic absences $0k0$ for $k = 2n + 1$ and $h0l$ for $h + l = 2n + 1$. The centrosymmetric monoclinic space group $P2_1/n$ is therefore uniquely defined.

Solution and refinement of the crystal structure calculations were carried out using the SHELXL program.[28] The structures were solved by direct methods and refined on F^2 by full-matrix least-squares techniques. The analytical scattering factors for neutral atoms were used throughout the analysis.[29]

For **1**, the dinuclear molecule is located about an inversion center. The geometry of the carbon atoms of the *tert*-butyl moiety was restrained during least-squares refinement. The *tert*-butyl carbons defined by C(8)−C(12), C(13)−C(17), and C(18)−C(22) were restrained (SAME[28]) by using carbon atoms C(3)−C(7) as the reference model. All hydrogen atoms were included using a riding model. At convergence, $wR2 = 0.2881$ and GOF = 1.035 for 143 variables refined against all 3623 unique data. As a comparison for refinement on F, $R1 = 0.0989$ for those 3052 data with which $F > 4.0\sigma(F)$. The high value obtained for $wR2$ is probably due in part to crystal decay and to high thermal motion. It was necessary to collect the data at room temperature because the crystal cracked at low temperatures (−90 to −120 °C).

For **2**, all of the hydrogen atoms were located from a difference Fourier map and included using a riding model. The molecule is a tetranuclear species and located about an inversion center. At convergence, $wR2 = 0.0988$ and GOF = 1.063 for 244 variables refined against all 2043 unique data. As a comparison for refinement on F, $R1 = 0.0377$ for those 1777 data with which $F > 4.0\sigma(F)$.

For **3**, the hydrogen atoms were located from a difference Fourier map and included with isotropic thermal parameters. The molecule is a dinuclear complex that located about an inversion center. At convergence, $wR2 = 0.1130$ and GOF = 1.069 for 213 variables refined against all 2060 unique data. As a comparison for refinement on F, $R1 = 0.0386$ for those 1821 data with which $F > 4.0\sigma(F)$.

Results and Discussion

We have recently reported two novel methods for the production of ferroelectric thin films of the perovskite phase of PMN[16,17] and PLZT[18,19] (Figure 1). Doping of the PZT material with niobium instead of lanthanum to form PNZT materials has also been realized using this new route.[18,19] Unfortunately, there are a limited number of suitable, well-characterized niobium alkoxides for use as starting materials to produce PMN or PNZT materials by these routes. $Nb(OEt)_5$ is the most common Nb source for solution routes; however, since this compound is an oil, the structure has not been determined. Therefore, to optimize the resulting PMN and PNZT materials by tailoring hydrolysis and condensation rates, we synthesized and characterized several sterically varied Nb alkoxide precursors, to be incorporated into our processes.

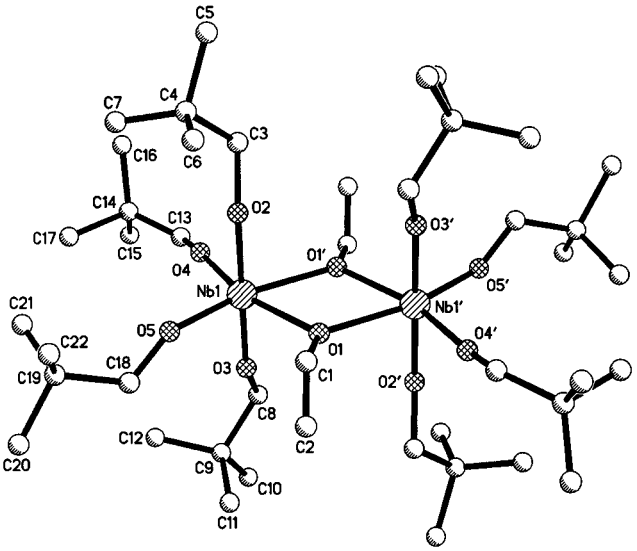

Figure 3. Ball-and-stick diagrams of $[Nb(\mu\text{-}OEt)(ONp)_4]_2$ (**1**).

Synthesis. Initial syntheses concentrated on reducing the number of reactive sites (i.e., terminal ligands) of $Nb(OEt)_5$. This was accomplished through the introduction of sterically hindering and/or multidentate ligands by the alcoholysis exchange route shown in eq 1. The alcohols used for this study included HONp, BHMP−H_3,[21] and THME−H_3 (see Figure 2).

$$Nb(OEt)_5 + xHOR \xrightarrow{\text{toluene}} Nb(OEt)_{5-x}(OR)_x + xHOEt \quad (1)$$

Excess HONp was added to $Nb(OEt)_5$ in toluene at elevated temperatures overnight. After removal of the volatile material followed by the appropriate washings, the remaining white powder was dissolved in hot toluene, and upon slow cooling, crystals of $[Nb(\mu\text{-}OEt)(ONp)_4]_2$ (**1**) were isolated. Figure 3 is a ball-and-stick diagram of **1**. It is of note that only four of the five OEt ligands of $Nb(OEt)_5$ were successfully metathesized. The analytical data of the bulk powder are consistent with the solid-state structure of **1**, further indicating that only partial exchange was obtained even at elevated temperatures. While the solubility of **1** is greatly diminished in comparison to $Nb(OEt)_5$, **1** is partially soluble at ambient temperatures in toluene and readily sublimed at ∼100 °C at 10^{-3} Torr.

To exchange the BHMP−H_3 for the OEt ligands in this system, elevated solution temperatures were required to increase the solubility of the BHMP−H_3 ligand. After heating overnight, the reaction mixture had turned a pale yellow color. Upon cooling, at −35 °C, X-ray-quality crystals of $[(\mu\text{-BHMP})Nb_2(\mu\text{-O})(OEt)_5]_2$ (**2**) were isolated, and their structure is shown in Figure 4. The elemental analysis of the bulk sample is consistent with the solid-state structure of **2**. A transesterification mechanism[30] between the BHMP and the ethoxide ligands would account for the generation of the observed oxide moiety.

$[(\mu\text{-THME})Nb(OEt)_2]_2$ (**3**) was easily isolated from the reaction mixture of THME−H_3 and $Nb(OEt)_5$. After stirring for 12 h at room temperature, the volume of the solution was drastically reduced and the reaction

(27) Braoch, R. W. Argonne National Laboratory, Illinois, 1978.
(28) (a) Sheldrick, G. M.; Program for Crystal Structure Refinement, University of Gottingen, Germany, 1993. (b) Sheldrick, G. M. Siemens Analytical X-ray Instruments Inc., 1994. (c) The SAME instruction restrains the bonds of the listed atoms to be the same length (with an esd) as those of the model atoms.
(29) *International Tables for X-ray Crystallography*; Dordrecht: Kluwer Academic Publishers, 1992; Vol. C.

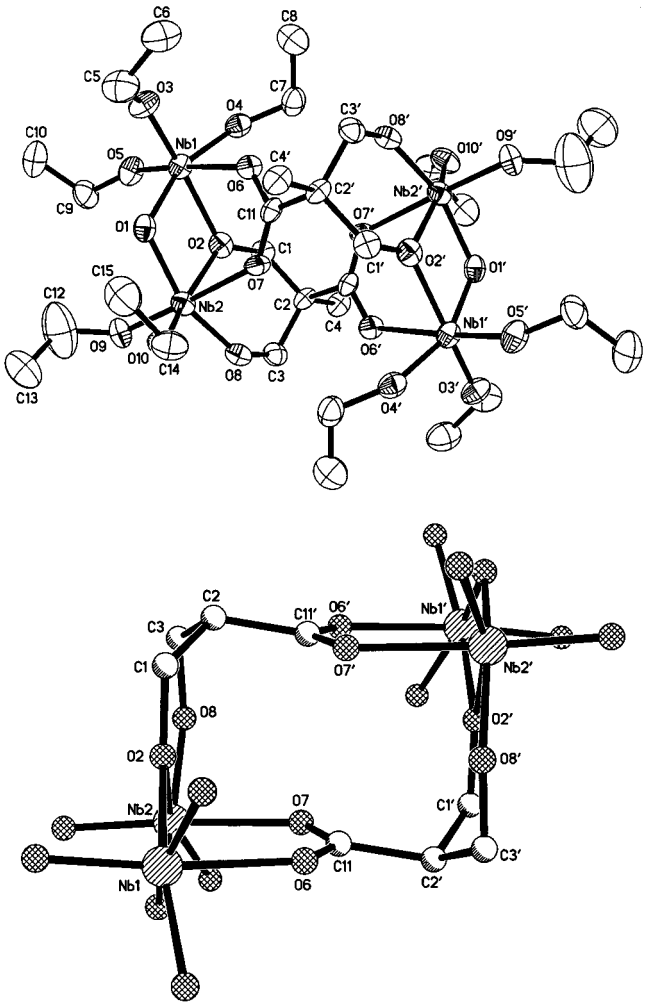

Figure 4. Thermal ellipsoid plot of (a, top) [(μ-BHMP)Nb_2-(μ-O)$(OEt)_5]_2$ (**2**, thermal ellipsoids are drawn at the 50% level) and (b, bottom) the central core of **2** (carbon and hydrogen atoms have been removed for clarity).

mixture was cooled to −35 °C. X-ray-quality crystals of **3** (see Figure 5) formed overnight. The bulk powder, obtained by removal of all volatile material from the reaction mixture, followed by a hexanes wash and toluene extraction, has an elemental analysis consistent with the crystal structure. The solubility of **3** is low in comparison to that of $Nb(OEt)_5$ but significantly higher than that of **1** or **2**. Surprisingly, **3** is *not* readily sublimable below 175 °C at 10^{-3} Torr. Above these conditions, a small fraction of the material was sublimed, which had analytical data consistent with that of **3**, as did the residual powder.

Solid-State X-ray Crystallographic Structures.[31−33] To our knowledge, only a few structures of homo- or heteroleptic alkoxy niobium(V) complexes have been reported;[31−35] these include $[Nb(OMe)_5]_2$,[36] $Nb_8O_{10}(OEt)_{20}$,[37] and of $[Nb(OCH_2SiMe_3)_5]_2$.[38] One could also

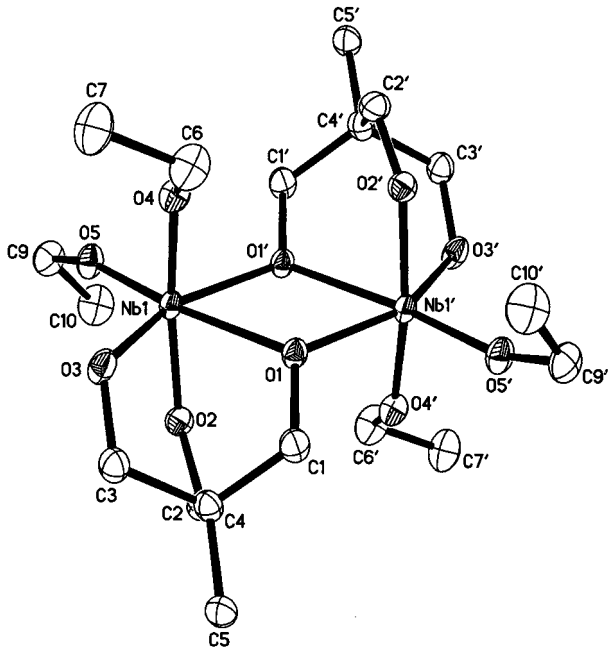

Figure 5. Thermal ellipsoid plot of and $[(\mu\text{-THME})Nb(OEt)_2]_2$ (**3**). Thermal ellipsoids are drawn at the 50% level.

include the aryl oxide complexes $Nb(OC_6H_4Me\text{-}4)_5$,[39] $Nb(OC_6H_3Me_2\text{-}3,5)_5$,[39] and $[Nb(O)(OC_6H_3(i\text{-}Pr\text{-}2,6)_3]_2$.[40] The remaining neutral Nb(V) species are a variety of mixed ligated compounds.[34,35,41−56] Due to the limited information on alkoxy niobium(V) complexes, single-

(30) Prabakar, S.; Assink, R. A.; Raman, N. K.; Brinker, C. J. *Mater. Res. Soc. Symp. Proc.* **1994**, *346*, 979.
(31) The Cambridge Structural Database was used for determination of structure types, literature references, bond distances, and bond angles.
(32) Allen, F. H.; Bellard, S.; Brice, M. D.; Cartwright, B. A.; Doubleday: A.; Higgs, H.; Hummelink, T.; Hummelink-Peters, B. G.; Kennard, O.; Motherwell, W. D. D.; Rodgers, J. R.; Watson, D. G. *Acta Crystllogr.* **1979**, *B35*, 146.
(33) Allen, F. H.; Kennard, O.; Taylor, R. *Acc. Chem. Res* **1983**, *16*, 146.
(34) *Comprehensive Organometallic Chemistry*; Wilkinson, G., Stone, F. G. A., Abel, E. W., Eds.; Pergamon Press: London, 1982; Vol. 3, Chapter 25, p 705.
(35) *Comprehensive Coordination Chemistry*; Wilkinson, G., Gillar, R. D., McCleverty, J. A., Eds.; Pergamon Press: London, 1987; Vol. 3, Chapter 34, p 585.
(36) Pinkerton, A. A.; Schwarzenbach, D.; Hubert-Pfalzgraf; Riess, J. G. *Inorg. Chem.* **1976**, *15*, 1196.
(37) Bradley, D. C.; Hursthouse, M. B.; Rodesiler, P. F. *Chem. Commun.* **1968**, 1112.
(38) Goel, S. C.; Hollingsworth, J. A.; Beatty, A. M.; Robinson, K. D.; Buhro, W. E. *Polyhedron* **1997**, *16*, in press.
(39) Coffindaffer, T. W.; Steffy, B. D.; Rothwell, I. P.; Folting, K.; Huffman, J. C.; Streib, W. E. *J. Am. Chem. Soc.* **1989**, *111*, 4742.
(40) Visciglio, V. M.; Fanwick, P. E.; Rothwell, I. P. *Acta Crystallogr., C (Cryst. Struct. Commun.)* **1994**, *50*, 900.
(41) Drew, M. G. B.; Rice, D. A.; Williams, D. M. *Inorg. Chim. Acta* **1986**, *118*, 165.
(42) Kirillova, M. I.; Gusev, A. I.; Pasynskii, A. A.; Struchkov, Y. T. *Zh. Strukt. Khim.* **1973**, *14*, 1075.
(43) Kalinnikov, V. T.; Pasynskii, A. A.; Larin, G. M.; Novotortsev, V. M.; Struchkov, Y. T.; Gusev, A. I.; Kirillova, N. I. *J. Organomet. Chem.* **1974**, *74*, 91.
(44) Jalon, F. A.; Otero, A.; Royo, P.; Fernadez; M., J.; Rosales, M. J.; Toscano, R. A. *J. Organomet. Chem.* **1987**, *331*, C1.
(45) Cotton, F. A.; Diebold, M. P.; Roth, W. J. *Inorg. Chem.* **1988**, *27*, 2347.
(46) Gosink, H. J.; Roesky, H. W.; Schmidt, H. G.; Noltemeyer, M.; Irmer, E.; Herbst-Irmer, R. *Organometallics* **1994**, *13*, 3420.
(47) Dahan, F.; Kergoat, R.; Tocquer, M. C.; Guerchais, J. E. *Acta Crystallogr., Sect B* **1976**, *32*, 1038.
(48) Bottomley, F.; Keizer, P. N.; White, P. S.; Preston, K. F. *Organometallics* **1990**, *9*, 1916.
(49) Corazza, F.; Floriani, C.; Chiesi-Villa, A.; Guastini, C. *J. Chem. Soc., Chem. Commun.* **1990**, 1083.
(50) Evans, D. F.; Slawin, A. M. Z.; Williams, D. J.; Wong, C. Y.; Woollins, J. D. *Polyhedron* **1993**, *12*, 1103.
(51) Chisholm, M. H.; Extine, M. *J. Am. Chem. Soc.* **1975**, *97*, 1623.
(52) Yu, J. S.; Fanwick, P. E.; Rothwell, I. P. *J. Am. Chem. Soc.* **1990**, *112*, 8171.
(53) Brown, D. A.; Wallbridge, M. G. H.; Li, W.-S.; Mcpartlin, M.; Scowen, I. J. *Inorg. Chim. Acta* **1994**, *227*, 99.
(54) Wailes, P. C. *J. Organomet. Chem.* **1976**, *76*, 119.
(55) Roskamp, E. J.; Pedersen, S. F. *J. Am. Chem. Soc.* **1987**, *109*, 6551.
(56) Okamoto, T.; Yasuda, H.; Makamura, A.; Kai, Y.; Kanahisa, N.; Kasai, N. *J. Am. Chem. Soc.* **1988**, *110*, 5008.

Table 2. Select Atomic Coordinates (×10⁴) and Equivalent Isotropic Displacement Parameters (Å² × 10³) for 1

atoms	*x*	*y*	*z*	*U*(eq)[a]
Nb(1)	4979(1)	630(1)	1295(1)	49(1)
O(1)	3979(6)	392(6)	−232(4)	47(1)
O(2)	3923(8)	−1145(8)	1035(6)	74(2)
O(3)	6142(7)	2371(7)	1592(6)	69(2)
O(4)	6211(9)	560(10)	2436(6)	83(2)
O(5)	3716(8)	1506(9)	1866(6)	76(2)

[a] *U*(eq) is defined as one-third of the trace of the orthogonalized U_{ij} tensor.

Table 3. Select Atomic Coordinates (×10⁴) and Equivalent Isotropic Displacement Parameters (Å² × 10³) for 2

atoms	*x*	*y*	*z*	*U*(eq)[a]
Nb(1)	7003(1)	4166(1)	1670(1)	29(1)
Nb(2)	4956(1)	3526(1)	244(1)	29(1)
O(1)	6542(4)	3501(2)	871(3)	30(1)
O(2)	5191(4)	4219(2)	1160(3)	31(1)
O(3)	8559(4)	4059(2)	1791(3)	38(1)
O(4)	7047(4)	4980(2)	2125(3)	34(1)
O(5)	6911(4)	3699(2)	2536(3)	39(1)
O(6)	6931(4)	4748(2)	639(3)	28(1)
O(7)	5455(4)	4355(2)	−329(3)	28(1)
O(8)	3437(4)	3848(2)	−52(3)	32(1)
O(9)	4609(4)	2796(2)	731(3)	37(1)
O(10)	4986(4)	3131(2)	−684(3)	40(1)

[a] *U*(eq) is defined as one-third of the trace of the orthogonalized U_{ij} tensor.

Table 4. Select Atomic Coordinates (×10⁴) and Equivalent Isotropic Displacement Parameters (Å² × 10³) for 3

atoms	*x*	*y*	*z*	*U*(eq)
Nb(1)	380(1)	1744(1)	146(1)	15(1)
O(1)	1429(3)	−300(3)	348(2)	17(1)
O(2)	204(3)	1442(3)	1425(2)	19(1)
O(3)	2568(3)	2338(3)	658(2)	22(1)
O(4)	968(3)	1780(2)	−1040(2)	22(1)
O(5)	−981(3)	3267(2)	−69(2)	22(1)

[a] *U*(eq) is defined as one-third of the trace of the orthogonalized U_{ij} tensor.

crystal X-ray studies were undertaken to verify the structures of these complex molecules.

Table 1 lists the data collection parameters for **1**−**3**. Tables 2−4 are the positional parameters of the heavier atoms for **1**−**3**, respectively. Table 5 shows a comparison of selected bond distances and angles for **1**−**3**. These compounds add to the family of crystallographically characterized niobium(V) alkoxides that consists solely of even-numbered compounds (2^n, n = integer) complexes: (a) $n = 1$: **1**, **3**, $[Nb(OMe)_5]_2$,[36] and $[Nb(OCH_2SiMe_3)_5]_2$;[38] (b) $n = 2$: **2**; (c) $n = 3$: $Nb_8O_{10}(OEt)_{20}$[37] unless sterically bulky ligands such as aryl oxides are invoked.[39,40]

$[Nb(\mu\text{-}OEt)(ONp)_4]_2$ (1). A ball-and-stick plot of **1** is shown in Figure 3. **1** was isolated in an edge-shared, bioctahedral, $M_2(\mu\text{-}X)_2(X)_8$ arrangement that is consistent with the only other crystallographically characterized niobium alkoxide compounds, $[Nb(OMe)_5]_2$[36] and $[Nb(OCH_2SiMe_3)_5]_2$.[38] The structure of **1** possesses a center of inversion, crystallizing in the $P2_1/n$ space group. Each Nb atom of **1** is octahedrally bound with oxygens, wherein, the OEt ligands adopt the bridging equatorial position and the ONp ligands fill the remaining coordination sites.

$[(\mu\text{-}BHMP)Nb_2(\mu\text{-}O)(OEt)_5]_2$ (2). Figure 4a is a thermal plot of compound **2** which is the first report of a metal complex involving the multidentate BHMP ligand. Compound **2** consists of two unsymmetrical "-$(EtO)_2Nb(\mu\text{-}O)Nb(OEt)_3$" moieties linked by two tetradentate BHMP ligands forming a rhombohedral shaped cagelike complex (Figure 4b). **2** was found to crystallize in the space group *C2/c* and therefore possesses a center of inversion relating the two halves. The dinuclear moieties of **2** possess two inequivalent octahedrally bound Nb atoms bridged by an oxide ligand and one methoxy fraction of the BHMP ligand. Interestingly, the bridging oxide ligand is forced to reside on the exterior of this dinuclear moiety, relatively unhindered by any ligands. The rest of the coordination sites are filled by the acetate-like portion of the BHMP moiety that binds an oxygen to each niobium metal center. One of the Nb atoms possesses three terminal ethoxide ligands. The other metal center uses two ethoxide ligands and the other methoxy BHMP moiety to complete its coordination sphere. Viewing the central core of **2** (Figure 4b) with the organic moieties of the ethoxide ligands and the methyl of the BHMP ligand removed, the central core encompasses a general void of 4.935 [the distance from the centroid of O(2′)−O(8′) to O(2)] by 3.354 Å [the centroid of O(6)−O(7) to C(11′)]. The synthetic strategy that produced compound **2** may be a potential synthetic route to compounds that contain systematically varied pore sizes, controlled by the dimensions of the BHMP ligand.

$[(\mu\text{-}THME)Nb(OEt)_2]_2$ (3). Compound **3** is the first THME ligated niobium compound reported. The THME ligand has been utilized in a number of other systems (Zubieta et al. have written a comprehensive review of polyoxomolybdates and vanadate structurally characterized compounds that contain these ligands[57]); however, only a few neutral, nonhalogenated, alkoxy complexes have been reported that incorporate this tridentate ligand.[20,58,59] For these uncharged, alkoxy, oxo species there are a large number of binding modes the THME ligand has been shown to adopt, including (a) both μ_3-O and μ-O as in $(\mu\text{-}THME)_2Ti_4(OCHME_2)_{10}$,[20] $[(\mu\text{-}THME)(MoO_2)_2(OEt)]_2$,[59] and $(\mu\text{-}THME)_3V_4O_4(OEt)_3$,[58] (b) only μ-O as in $(\mu\text{-}THME)_2Zr_4(OCHMe_2)_{10}$,[20] (c) one μ-O and one O_{term} on two different metal centers as in $(\mu\text{-}THME)_2V_4O_4(OMe)_6$,[58]and (d) chelating with one μ-O and two O_{term} oxygens as is found for the $[(\mu\text{-}THME)MoO(OEt)]_2$ complex.[59] The structure of the dinuclear species **3** (shown in Figure 5) is an edge-shared bioctahedron that crystallized in the $P2_1/n$ space group in an analogous arrangement as reported for the $[(\mu\text{-}THME)MoO(OEt)]_2$ compound.[59] Compound **3** is the simplest binding mode observed for the THME ligand for a purely alkoxide system (the Mo system involves oxo ligands) and can be thought of as another example of the $M_2(\mu\text{-}X)_2(X)_8$ structure type. A center of inversion relates the two halves of this complex where each Nb is octahedrally bound by oxygen atoms. Two of these oxygens are from terminal ethoxide ligands in an axial and equatorial position; wherein, the rest are from a chelating THME ligand. One of the equatorial THME oxygens

(57) Chen, Q.; Zubieta, J. *Coord. Chem. Rev.* **1992**, 107.
(58) Crans, D. C.; Jiang, F.; Chen, J.; Anderson, O. P.; Miller, M. M. *Inorg. Chem.* **1997**, *36*, 1038.
(59) Mckee, V.; Wilkins, C. J. *J. Chem. Soc., Dalton Trans.* **1987**, 523.

Table 5. Comparison of the Interatomic Distances (Å) and Angles (deg) for 1−3

distances (Å)	**1**[a]		**2**[b−d]		**3**[e]	
Nb- - -Nb	3.516		Nb(1)- - -Nb(2)	3.241	3.459	
Nb−(OR)	Nb(1)−O(2)	1.901(7)	Nb(1)−O(3)	1.866(5)	Nb(1)−O(4)	1.904(3)
	Nb(1)−O(3)	1.903(7)	Nb(1)−O(4)	1.881(5)	Nb(1)−O(5)	1.860(3)
	Nb(1)−O(4)	1.889(7)	Nb(1)−O(5)	1.868(5)		
	Nb(1)−O(5)	1.885(6)	Nb(2)−O(9)	1.875(5)		
			Nb(2)−O(10)	1.892(5)		
Nb−(OL)			Nb(1)−O(6)	2.189(4)[d]	Nb(1)−O(2)	1.926(3)
			Nb(2)−O(7)	2.199(5)[d]	Nb(1)−O(3)	1.935(3)
			Nb(2)−O(8)	1.892(5)[c]		
Nb−(*μ*-OL)	Nb(1)−O(1)	2.135(6)	Nb(1)−O(2)	2.120(5)[c]	Nb(1)−O(1)	2.170(2)
	Nb(1)−O(1′)	2.143(6)	Nb(2)−O(2)	2.138(4)[c]	Nb(1)−O(1′)	2.086(2)
Nb−(*μ*-O)			Nb(1)−O(1)	1.945(5)		
			Nb(2)−O(1)	1.911(5)		

angles (deg)	**1**[a]		**2**[b−d]		**3**[e]	
Nb−O−C_{term}	Nb(1)−O(5)−C(18)	145.8(1)	Nb(1)−O(3)−C(5)	141.5(5)	Nb(1)−O(4)−C(6)	138.0(3)
	Nb(1)−O(3)−C(8)	152.5(7)	Nb(1)−O(4)−C(7)	145.3(4)	Nb(1)−O(5)−C(9)	156.7(3)
	Nb(1)−O(2)−C(3)	152.8(8)	Nb(1)−O(5)−C(9)	150.7(5)		
	Nb(1)−O(4)−C(13)	170(2)	Nb(2)−O(9)−C(12)	141.4(7)		
			Nb(2)−O(10)−C(14)	144.9(5)		
Nb−O−L_{term}			Nb(2)−O(7)−C(11)	129.0(4)[d]	Nb(1)−O(2)−C(2)	128.8(2)
			Nb(1)−O(6)−C(11)	131.6(4)[d]	Nb(1)−O(3)−C(3)	125.6(2)
			Nb(2)−O(8)−C(3)	139.4(4)[c]		
Nb−(*μ*-O)−Nb			Nb(2)−O(1)−Nb(1)	114.4(2)		
Nb−(*μ*-OL)−Nb	Nb(1)−O(1)−Nb(1′)	110.6(2)	Nb(1)−O(2)−Nb(2)	99.1(2)[c]	Nb(1)−O(1)−Nb(1′)	108.7(1)
Nb−(*μ*-O)−C	Nb(1)−O(1)−C(1)	123.0(9)	Nb(2)−O(2)−C(1)	133.0(4)	Nb(1)−O(1)−C(1)	119.7(2)
	Nb(1′)−O(1)−C(1)	124.1(9)				
O−Nb−O	O(2)−Nb(1)−O(3)	176.2(3)	O(3)−Nb(1)−O(5)	100.1(2)	O(2)−Nb(1)−O(4)	167.1(1)
	O(2)−Nb(1)−O(4)	88.9(4)	O(9)−Nb(2)−O(10)	97.2(2)	O(4)−Nb(1)−O(5)	96.3(1)
	O(2)−Nb(1)−O(5)	90.4(4)				
O−Nb−(*μ*-O)	O(1)−Nb(1)−O(4)	162.7(3)	O(1)−Nb(1)−O(4)	158.0(2)	O(1)−Nb(1)−O(2)	81.2(1)
	O(1′)−Nb(1)−O(5)	162.9(3)	O(2)−Nb(1)−O(3)	161.9(2)	O(1)−Nb(1)−O(3)	83.7(1)
	O(2)−Nb(1)−O(1)	90.6(3)	O(5)−Nb(1)−O(6)	174.4(2)	O(1)−Nb(1)−O(4)	87.6(1)
	O(2)−Nb(1)−O(1′)	89.3(3)	O(1)−Nb(2)−O(8)	154.4(2)	O(1)−Nb(1)−O(5)	166.3(1)
			O(2)−Nb(2)−O(10)	161.2(2)	O(1′)−Nb(1)−O(3)	155.0(1)
			O(7)−Nb(2)−O(9)	176.7(2)		

[a] OR = OCH_2CMe_3 and OL = OCH_2Me. [b] OR = OCH_2Me. [c] OL = $MeC(CH_2\mathbf{O})_2(C(O)O)$. [d] OL = $MeC(CH_2O)_2(C(\mathbf{O})\mathbf{O})$. [e] OR = OCH_2Me and OL = $MeC(CH_2O)_3$.

acts as a unidentate bridge to form a standard edge shared dinuclear complex.

Metrical Data. Select bond distances and angles of **1**−**3** are shown in Table 5. Due to the limited number of crystallographically characterized Nb alkoxide complexes,[36,37] comparison of metrical data from other homoligated niobium alkoxide complexes is difficult. As is typically observed for transition metals, bond lengths aggrandize with the degree of binding (OR_{term} < *μ*-OR < μ_3-OR) independent of the residual group of the ligand;[20,60] however, the tridentate ligands do have longer Nb−O bond lengths (av 1.92 Å) than the terminal ethoxide ligands (av 1.88 Å). This has been observed in other similarly tridentate ligated systems.[20] These distances are all consistent with various literature reports on heteroligated Nb(V) compounds.[31−37,39−56,61−64] The Nb−(*μ*-OR) distances and the (*μ*-O)−Nb−(*μ*-O) angles [**1** (69.4°), **2** (72.9°), and **3** (71.3°)] are approximately the same for the three compounds. Furthermore, **1** and **3** have nearly identical nonbonding Nb- -Nb distances (3.516 and 3.459 Å, respectively) in agreement with the OMe structure; whereas for **2** the M- -M distance is significantly reduced to 3.241 Å, an indication of the geometrical constraints imposed by the oxide and acetate-like moiety of the BHMP ligand. The longest M−(*μ*-O) distance noted for these compounds is observed for **3**, at 2.17 Å. The length of this bond must be a result of the steric repulsion between the bridging THME ligands.

For **1**, the overall average bond lengths and angles for the molecule are consistent with the reported [Nb(OMe)$_5$]$_2$ complex.[36] It is of note that for **1** there is no distortion in the axial ligand Nb−O−C bonds (average 152.6°) as was observed for the OMe derivative; however, the equatorial ligands do show a significant difference in this angle 170.0° for C(13) to 145.8° for C(18). As observed for the [Nb(OMe)$_5$]$_2$ complex, no significant trans effect (equatorial Nb−O bond lengths being shorter than the axial ones) was observed for **1**.[36]

For **2**, the M−(*μ*-O) ligand distance (av 1.93 Å) is shorter than the M−(*μ*-OR) acetate (av 2.19) and alkoxy (av 2.13 Å) moieties of the BHMP ligand. The M−OR distance of the BHMP ligand (1.87 Å) is in agreement with the terminal M−OEt ligand distances (av 1.88). The angle of ∼126° for the acetate moiety of the BHMP ligand O(6)−C(11)−O(7) of **2** is within the range reported for other niobium complexes with some form of acetate ligand.[45,51,61,63,64]

FT-IR Spectroscopy. The FT-IR spectra were obtained for Nb(OEt)$_5$ (neat, NaCl plates) and the resulting powders of **1**−**3** (KBr pellet). Even though there are a variety of alkoxide ligands present, each compound has stretches consistent with terminal alkoxide ligands as well as one peak at ∼920 cm^{-1} representative of Nb−(*μ*-O)−C.[65] This stretch is extremely small but still present in the spectrum of **1**.

(60) Boyle, T. J.; Bradley, D. C.; Hampden-Smith, M. J.; Patel, A.; Ziller, J. W. *Inorg. Chem.* **1995**, *34*, 5893.

The FT-IR spectra of **1**−**3** and $Nb(OEt)_5$ are very similar since the resulting compounds possess OEt ligands and the basic constructs of their other pendent ligands (ONp, BHMP, and THME) have similar components in comparison to the OEt ligand. For **1**, the characteristic four peak stretches associated with ONp ligands are present in the alkane region around 3000 cm^{-1}; however, there is a slight distortion of these stretches due to the presence of the bridging ethoxide ligands. For **2** there is a sharp stretch at 1560 cm^{-1}. Acetates are known to adopt several coordination modes, including monodentate, chelating, and bridging. Literature reports show the acetate ligands of Nb(V) compounds appear around 1600 to 1550 cm^{-1}.[41,45,51,61,63−65] Therefore, this peak has been assigned as the bridging BHMP acetate, significantly shifted from the free BHMP (1690 cm^{-1}). The M−O region is extremely complex with a sharp peak around 700 cm^{-1} that does not appear in any of the other spectra and has been associated with the Nb−(μ-O)−Nb moiety.[65,66] The FT-IR spectrum of the crystalline material of **3**, in contrast to the oil $Nb(OEt)_5$, has a much sharper M−O−C and M−O region; otherwise the two spectra are very similar.

TGA/DTA Analysis. TGA/DTA spectra were obtained on **1**−**3** under an atmosphere of oxygen to ensure complete conversion to the metal oxide. XRD analysis of the fired powders showed that each sample was fully converted to Nb_2O_5 after sintering to 650 °C. The TGA spectra show actual (theoretical) weight losses of 55.2 (72.7) for **1**, 55.2 (52.5) for **2**, and 42.0 (55.7) % for **3**. Small endotherms are present at low temperatures (<175 °C), consistent with melting of the crystalline material. All the remaining TGA events are exothermic with an appropriate weight loss shown in the DTA. For **1**, the organic weight loss occurs before 300 °C in the TGA coupled with a large exothermic peak in the DTA. This is followed by a small final weight loss step concurrent with a minor crystallization exotherm. While the mismatch between experimental and theoretical results of **1** is not fully understood to date, ligand hydrolysis due to ambient humidity may account for this differential. For **2** and **3**, there are two large exothermic events at ∼300 °C; however, the exotherms of **2** are much broader and ∼4.5 times smaller than those of **3**. Furthermore, both spectra show high-temperature exotherms (∼535 °C) associated with the conversion from amorphous to crystalline material, but the peak for **3** is significantly smaller than that observed for **2**. This is most likely due to the large exotherms resulting from the low-temperature ligand loss of **3** that also initiates "low-temperature" crystallization of the Nb_2O_5. This rapid burning causes material loss due to "bumping", explaining the small variation between theoretical and experimental results. The temperature for complete organic combustion of these compounds was **3** (569 °C) < **1** (581 °C) < **2** (586 °C). This indicates that the higher nuclearity species require higher processing temperatures.

Solution-State Molecular Weight Determination. Due to the low solubility of **1** and **2** at room temperature in both toluene and CH_3Cl, standard molecular weight (MW) studies (Signer method)[67] to determine the nuclearity of these new alkoxides in solution could not be undertaken. The room-temperature MW of **3**, in toluene was found to be ∼750. This implies a molecular weight of ∼1.25 times the solid-state structure or a molecular complexity of 2.5 indicating the presence of higher order molecular species in solution. This value is significantly higher than that observed for $Nb(OEt)_5$ (av 1.89[68] or 2.02[65]).

^{1}H and ^{13}C NMR Spectroscopy. All of the NMR spectra for **1**−**3** were obtained by redissolution of crystalline material in toluene-d_8, unless otherwise noted. The samples were prepared as concentrated as possible (a small insoluble amount of crystalline material was present for each sample prepared). There was no observable change in the ^{1}H NMR solution spectra over a 3 month period of time. Low-temperature NMR experiments were not undertaken for **1** or **2** due to their low solubility.

A number of broad multiplets for the OEt and ONp ligands were observed in toluene for **1**, the ratio of which changes based on the concentration of the sample. Slightly elevated temperatures (310−315K) yielded spectra with sharper peaks. This may be representative of a high degree of dynamic behavior, due to rapid alkoxy exchange and a multinuclear equilibrium, (eq 2).[65] This multinuclear equilibrium was further borne

$$2Nb(OR)_5 \rightleftarrows Nb_2(OR)_{10} \rightleftarrows {}^2/_3Nb_3(OR)_{15} \rightleftarrows {}^1/_2Nb_4(OR)_{20} \quad (2)$$

out by ^{93}Nb NMR investigations (vide infra). For **1** in $CDCl_3$, one broad methyl resonance for the ONp, one broad resonance for the OEt ligands, and a multiplet of methylene peaks were observed. The elevated temperature ^{13}C NMR spectrum of **1**, in either solvent, also reveals the presence of OEt and ONp ligands. On the basis of the spectra recorded for **1**, it is apparent that an equilibrium coupled with rapid alkoxy exchange is occurring.

For **2**, the ^{1}H NMR spectrum obtained on the crystalline material was very complex but does appear to be in agreement with the solid-state structure. There are two regions around 4.5 and 1.0 ppm, representing the methylene and methyl resonances, respectively, of the BHMP and OEt ligands. Of the six methylene resonances present, four are doublets associated with the four inequivalent methylene BHMP protons and two are broad multiplets in an ∼2:3 ratio assigned as the inequivalent methylene protons of the ethoxide ligand. The methyl resonances consist of two broad peaks representing the inequivalent methyls of the ethoxide, and one sharp peak for the BHMP methyl. The ^{1}H spectrum is consistent with retention of the solid-state structure in solution. Further evidence for this retention is observed in the ^{13}C NMR spectrum where there

(61) Cotton, F. A.; Diebold, M. P.; Matusz, M.; Roth, W. J. *Inorg. Chim. Acta* **1986**, *112*, 147.
(62) Dahan, F.; Kergoat, R.; Senechal-Tocquer, M. C.; Guerchais, J. E. *J. Chem. Soc., Dalton Trans.* **1976**, 2202.
(63) Pasynskii, A. A.; Skripkin, Y. V.; Eremenko, I. L.; Kalinnikov, V. T.; Aleksandrov, G. V.; Struchkov, Y. T. *J. Organomet. Chem.* **1979**, *39*, 39.
(64) Lecomte, C.; Protas, J.; Guilard, R.; Fliniaux, B.; Fournari, P. *J. Chem. Soc., Dalton Trans.* **1979**, 1306.
(65) Bradley, D. C.; Mehrotra, R. C.; Gaur, D. P. *Metal Alkoxides*; Academic Press: New York, 1978.
(66) Lu, Y. J.; Lalancette, R.; Beer, R. H. *Inorg. Chem.* **1996**, *35*, 2524.
(67) Clark, E. P. *Anal. Ed.* **1941**, 820.

are clearly 10 inequivalent resonances associated with the methyl and methylene carbons of the OEt ligands as well as 5 resonances for the carbons of the BHMP ligands.

For **3**, the ^{1}H and ^{13}C NMR spectra are consistent with a highly symmetric molecule being present in solution. The ^{1}H NMR of **3** displays resonances at δ 4.38 (bridging methylene), δ 4.23 (terminal methylene), and δ 0.33 (methyl) for the THME ligand along with ethoxide resonances at δ 4.54 (methylene) and δ 1.24 (methyl). The ^{13}C NMR spectrum reveals six resonances that have been assigned as the OCH_2 bridging (δ 83.7), OCH_2 chelating (δ 82.7), quaternary (δ 48.3), and methyl (δ 19.7) carbons of the THME ligand and methylene (δ 74.1) and methyl (δ 25.0) resonances for the carbons of the ethoxide ligands. There are two inequivalent methylene resonances (bridging vs terminal) present for the THME ligands indicating that the solid-state structure of **3** was retained in solution. A high-temperature (>360 K) NMR spectrum showed no change in the recorded ^{1}H NMR spectrum of **3**. At low temperature (233 K), the coalescence of the THME methylene resonances into one broad peak was recorded. Reducing the temperature to 193 K revealed two types of ethoxide ligands and complete separation of the methylene resonances. Throughout this temperature range only one methyl for the THME ligand was noted. These spectra suggest that the OEt ligands are in rapid exchange but that the general solid-state structure is retained in solution; however, the molecular weight study indicates that some form of equilibrium with higher order oligomers is occurring (eq 2) in solution.

On the basis of the ^{1}H and ^{13}C NMR studies, $Nb(OEt)_5$, **1**, and **3** undergo some form of rapid ligand exchange in toluene, while **2** retains its solid-state structure in solution. Therefore, an alternative nucleus (^{93}Nb) was investigated using NMR spectroscopy to further elucidate the solution behavior of these compounds.

^{93}Nb NMR Spectroscopy. Despite the fact that the ^{93}Nb nucleus has 100% natural abundance and an acceptable sensitivity of 0.49 (^{1}H = 1.0), its large quadruple moment (-2.8×10^{-29} m^2), and spin of $^9/_2$ cause broad signals to be observed and therefore limits its use to highly symmetric compounds.[69] However, a number of reports that utilize ^{93}Nb NMR to characterize a wide range of Nb(V) compounds can be found in the literature,[66,68−89] some of which focused on the characterization of niobium alkoxide species.[69,77,80,81]

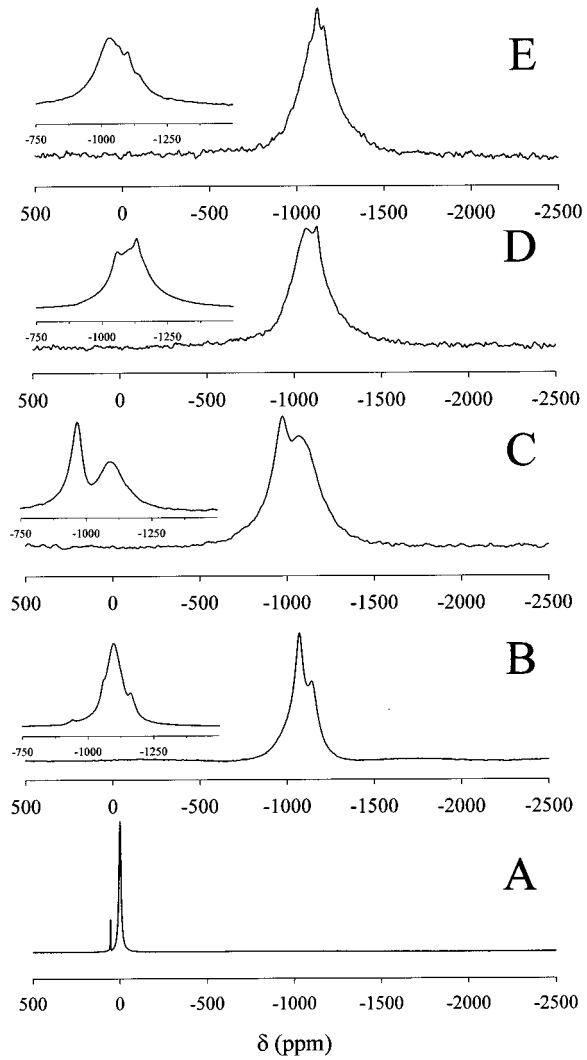

Figure 6. Solution ^{93}Nb NMR (298 K, toluene-d_8) spectra of (a) $NbCl_5(CH_3CN)$, (b) $Nb(OEt)_5$, (c) **1**, (d) **2**, and (e) **3**. Insert spectra are at 380 K.

Figure 6 is a plot of the ^{93}Nb solution spectra of $NbCl_5$ in CH_3CN,[69] $Nb(OEt)_5$, and **1**−**3** in toluene-d_8 at room temperature while the insets are the spectra obtained at elevated temperature (380 K). If the solid-state structures of these compounds were retained in solution, only one resonance should be observed for $Nb(OEt)_5$, **1**, and **3** and two peaks for **2**; however, for each compound, multiple, extremely broad ^{93}Nb resonances were ob-

(68) Bradley, D. C.; Chakravarti, B. N.; Wardlaw, W. *J. Chem. Soc.* **1956**, 2381.
(69) Rehder, D.; Rodewald, D. In *Advanced Applications of NMR to Organometallic Chemistry*; Gielen, M., Willem, R., Wrackmeyer, B., Eds.; John Wiley & Sons Ltd.: New York, 1996; pp 304−311.
(70) Blumel, J.; Born, E.; Metzger, T. *Phys. Chem. Solids* **1994**, *55*, 589.
(71) Brunner, H.; Gehart, G.; Meier, W.; Wachter, J.; Wranckmeyer, B.; Nuber, B.; Zielgler, M. L. *J. Organomet. Chem.* **1992**, *436*, 313.
(72) Butaud, P.; Segransan, P.; Berthier, C.; Meershaut, A. *Lecture Notes Phys.* **1985**, *217*, 121.
(73) Calderazzo, F.; Felten, C.; Pampaloni, G.; Rehder, D. *J. Chem. Soc., Dalton Trans.* **1992**, *11*, 3073.
(74) Catchen, G. L.; Spaar, D. M. *Phy. Rev. B, Condens. Mater.* **1991**, *44*, 12137.
(75) Cheathan, L. K.; Graham, J. J.; Apblett, A. W.; Barron, A. R. *Polyhedron* **1991**, *10*, 1075.
(76) Davis, J.; Tinet, D.; Fripiat, J. J.; Amarilla, J. M.; Casal, B.; Ruizhitsky, E. *J. Mater. Res.* **1991**, *6*, 393.
(77) Eichorst, D. J. Ph.D. Thesis, University of Illinois at Urbana−Champaign, 1991.
(78) Felten, C.; Rodewald, D.; Priebsch, W.; Olbrich, F.; Rehder, D. *J. Organomet. Chem.* **1994**, *480*, 51.
(79) Kohori, Y.; Kohara, T.; Oda, Y.; Nishikawa, M.; Kita, E.; Tasaki, A. *Physica B* **1994**, *194*, 2383.
(80) Lee, G. R.; Crayson, J. A. *J. Chem. Soc., Dalton Trans.* **1991**, *11*, 3073.
(81) Norcross, J. A.; Ailion, D. C.; Blinc, R.; Dolinsek, J.; Apih, T.; Slak, J. *Phys. Rev. B, Condens. Mater.* **1994**, *6*, 393.
(82) Rempel, A. A.; Gusev, A. I.; Belyaev, M. Y. *J. Phys. C, Solid State Phys.* **1987**, *20*, 5655.
(83) Ren, J.; Whangbo, M. H. *Phys. Rev. B, Condens. Mater.* **1992**, *46*, 4917.
(84) Skripov, A. V.; Sibirtsev, D. S.; Cherepanov, Y. G.; Aleksashin, B. S. *J. Phys., Condens. Mater.* **1994**, *7*, 4479.
(85) Yatsenko, A. V.; Sergeev, N. A. *Ukran. Fis. Z.* **1988**, *33*, 1101.
(86) Yatsenko, A.; Ivanova, E. *Fiz. Tverdogo Tela* **1995**, *37*, 2262.
(87) Yatsenko, A. V.; Sergeev, N. A. *Dokl. Akad. Nauk Ukran. RSR Ser.* **1985**, *12*, 57.
(88) Yogo, T.; Kikuta, K.; Ito, Y.; Hirano, S. *J. Am. Ceram. Soc.* **1995**, *78*, 2175.
(89) Sanchez, C.; Toledano, P.; Ribot, F. *Mater. Res. Soc. Symp. Proc.* **1990**, *180*, 47.

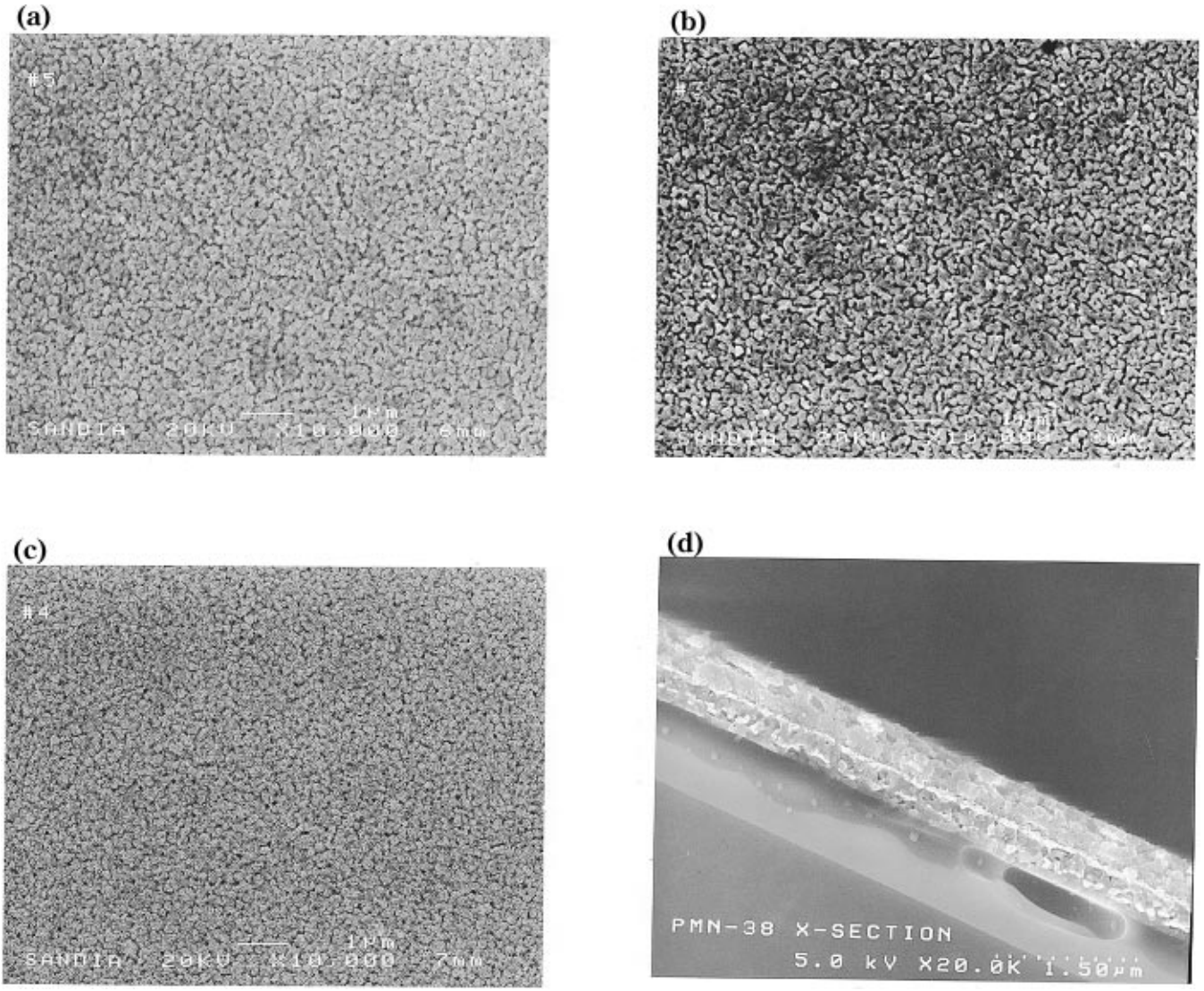

Figure 7. Scanning electron micrographs of PMN films produced using (a) $Nb(OEt)_5$, (b) **1**, (c) **3**, and (d) side view.

Table 6. Solution ^{93}Nb NMR (Toluene-d_8) at 298 and 380 K of the Observed Chemical Shifts of $Nb(OEt)_5$ (1−3)

	δ (ppm)	
compound	298 K	380 K
$Nb(OEt)_5$ (toluene)	−1070	−941
	−1142	−1059
		−1099
		−1163
1	−967	−964
	−1054	−1095
2	−1081	−1058
	−1131	−1104
		−1132
3	−1065	−1032
	−1113	−1063
	−1151	−1098
		−1137

served. Due to the complex solution behavior only the observed ^{93}Nb chemical shifts are reported (Table 6). These resonances range from approximately −900 to −1200 ppm at both 298 and 380 K and are significantly higher in frequency in comparison to other Nb(V) compounds reported.[69] However, they are in agreement with the chemical shifts reported for the $[Nb(OMe)_5]_2$ and $NbCl_{5-x}(OR)_x$ (x = 1−5; R = Me) compounds investigated by Lee and Crayston.[80]

Why these multinuclear interactions (eq 2) were not readily observed in the standard ^{1}H and ^{13}C NMR spectra can be explained by the fact that the ^{93}Nb line widths are very large, ranging from ∼6000 to 21 000 Hz at room temperature and peak separations of ∼7000 Hz. For molecular exchange to produce a single averaged resonance, the exchange rate needs to be faster than the peak separation. The peak separation expected for ^{1}H and ^{13}C due to changes in oligomerization would only be on the order of ∼100−500 Hz, much smaller than that observed for ^{93}Nb nucleus. The molecular exchange rate required to motionally average ^{1}H and ^{13}C spectra are therefore significantly lower than those required for ^{93}Nb. This difference in time scales is one of the benefits of employing ^{93}Nb NMR as a tool to probe solution complexation behavior.

Film Processing. Films of PMN and PNZT (where N = $Nb(OEt)_5$, **1**, and **3**) were all generated by standard spin-cast deposition methods in air.[17,18,20,90] The low solubility of **2** did not allow for the generation of a uniform solution for either the PMN or PNZT precursor solutions; so, use of this precursor was not pursued further.

$Pb(Mg_{0.33}Nb_{0.66})O_3$. Figure 1a is a schematic representation of the general PMN precursor preparation we have developed.[16,17] The precursor solution consists

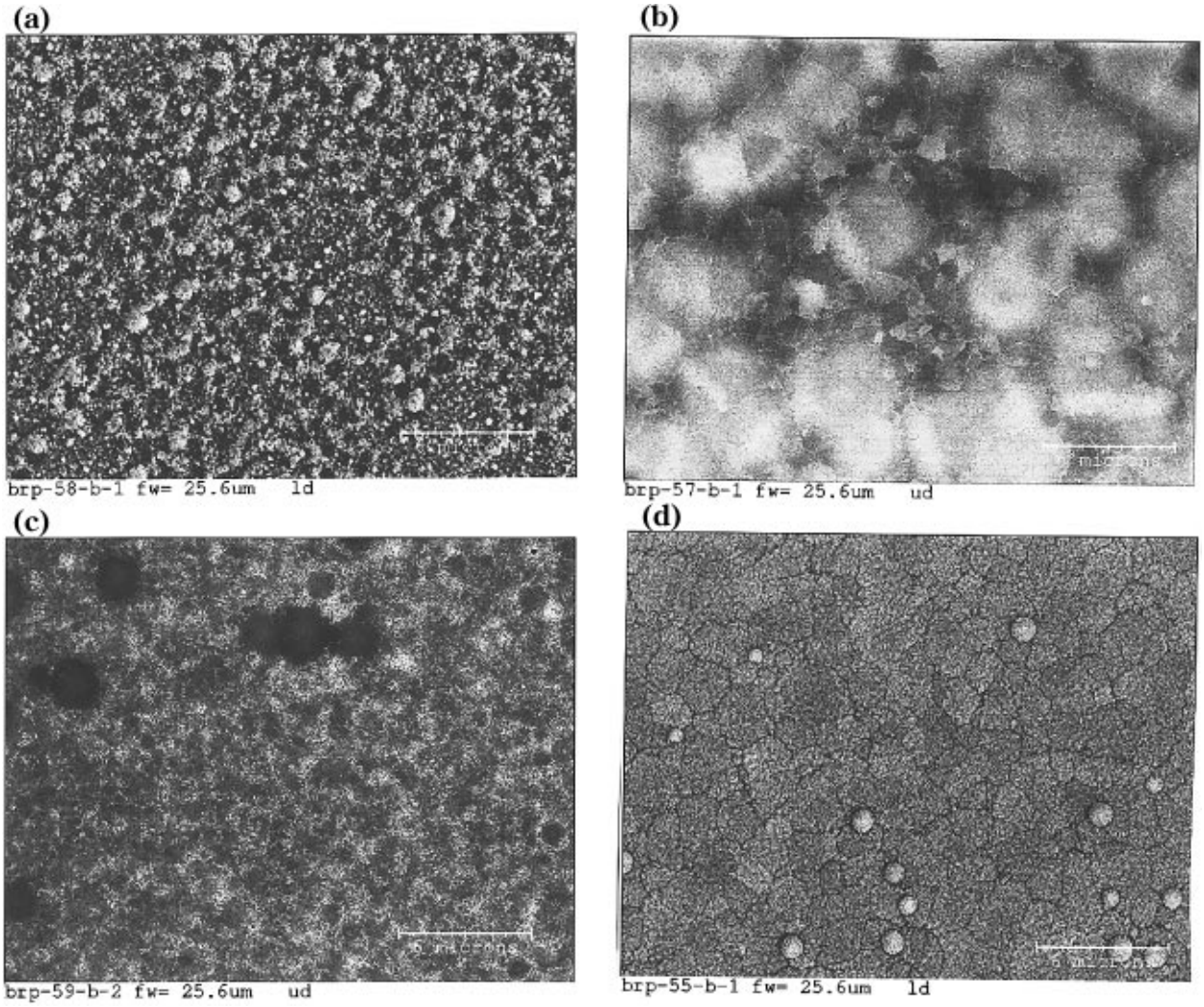

Figure 8. Scanning electron micrographs of PNZT films produced using (a) $Nb(OEt)_5$, (b) **1**, (c) **3** and (d) "$Nb(OAr'')_5$".

of a mixture of Pb:Mg:Nb in a ratio of 1.1:0.33:0.66 (excess lead was utilized to compensate for lead loss during processing). All precursors were individually soluble in toluene; however, **1** and **3** require heating to solubilize the starting material at the desired molarity. $Mg(n\text{-}Bu)_2$ was added to the premixed Pb/Nb solution, whereupon the reaction mixture immediately turned to a dark brown color. XRF studies of the precipitate showed this to be Pb^0 which is filtered out of solution before deposition. Figure 7 shows the SEM micrographs of the PMN films produced using the niobium complexes $Nb(OEt)_5$, **1**, and **3** in our system.

Before firing, the PMN films appeared transparent with few or no defects; however, after heat treatment, the films developed a hazy appearance and roughness due to a large number of voids and cracks. Grazing incidence X-ray diffraction analysis of these films shows each to be phase pure perovskite with a slight negative shift in the 2θ of the unit cell. This shift is most likely caused by compression of the material through stress induced by the Pt surface.[91] SEM micrographs of these films, shown in Figure 7, were obtained to characterize any microstructural differences in these films. The surface uniformity of the resultant films followed the general trend of $Nb(OEt)_5$ < **1** < **3** that is consistent with the number of readily hydrolyzable ligands. The initial films using $Nb(OEt)_5$ or **1** produced films that were nearly identical in microstructure, which is not surprising based on the structural similarities of these compounds. The surface appears rough but is very uniform with submicron crystallites and densely packed layers. There appears to be some pyrochlore present at the surface that may be due to lead loss at the exposed surface. Introduction of **3**, markedly reduced observable microstructural cracks and voids in comparison to **1**. The densities of the films were increased as well. Side views of these films (Figure 7d) show horizontal layers and reveal porosity throughout the film. Even in multilayered films, the interconnected nature of the porosity is apparently sufficient to generally cause electrical shorting between the sputtered top electrode metal and the continuous bottom electrode. Consequently, successful characterization of the dielectric properties of perovskite PMN films have been achieved in only a couple of cases where an effective permittivity of $\epsilon = 800-1000$ has been obtained. This is substantially lower than the best values previously reported ($\epsilon > 2000$).[11] The presence of porosity and the possibility of some residual pyrochlore at the surface could be responsible for the reduced permittivity.

$Pb(Nb_{0.05}(Zr_{0.4}Ti_{0.6})_{0.95})O_3$. Figure 1b is a schematic representation of the general PNZT precursor preparation.[18,19] A typical synthesis involves mixing two solutions—$Pb(O_2CMe)_4$ in pyridine with $[Zr(OCHMe_2)_4 \cdot HOCHMe_2]_2$ and $Ti(OCHMe_2)_4$ in toluene—excess lead was utilized to compensate for lead loss during process-

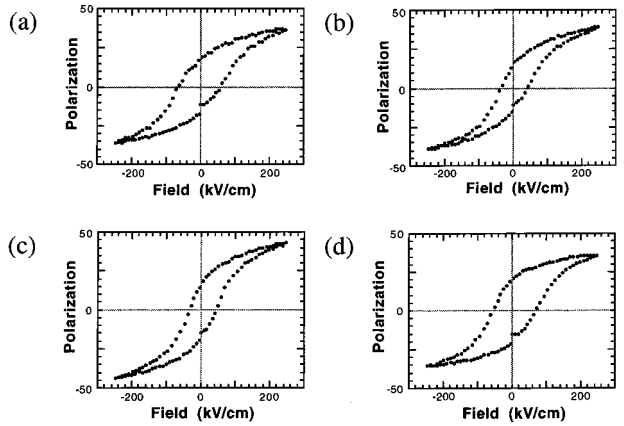

Figure 9. Hysteresis loops of PNZT films produced using (a) $Nb(OEt)_5$, (b) **1**, (c) **3** and (d) "$Nb(OAr'')_5$".

Table 7. Ferroelectric Results for Pt||PNZT(4/50/50)||Pt Capacitors[a] Using (a) $Nb(OEt)_5$, (b) 1, (c) 3, (d) "$Nb(OAr'')_5$"

dopant	P_r (av) ($\mu C/cm^2$)	P_s ($\mu C/cm^2$)	V_c (av) (V)	ϵ	dissipation factor
$Nb(OEt)_5$	18.37	36.40	4.96	981	0.072
1	16.15	39.15	3.04	1800	0.027
3	18.92	43.49	3.19	1720	0.032
$Nb(OAr'')_5$	21.03	35.67	4.99	876	0.04

[a] Films were ~5000 Å in thickness with 20 V applied for P_r and P_s measurements. Top Pt electrodes were shadow mask deposited dots, ~150 μm in diameter.

ing. Once this solution clears (<5 min) the Nb dopants are added. All precursor solutions were soluble and required no heating to generate a uniform solution. Films were made with the following Nb dopants: $Nb(OEt)_5$, "$Nb(OAr'')_5$" [$OAr'' = OC_6H_3(2,6\text{-}CHMe_2)$],[39,40] **1**, and **3**. Figure 8 shows the SEM of the resulting films of $Nb(OEt)_5$, **1**, "$Nb(OAr'')_5$", and **3**. The hysteresis loops of these films as Pt//PNZT//Pt capacitors are shown in Figure 9, and their properties are listed in Table 7. The values obtained on these films are comparable, if not superior, to other films generated by traditional routes at higher temperatures.

The uniformity of the films correlates with the number of readily hydrolyzable ligands: $Nb(OEt)_5$ < **1** < **3** < "$Nb(OAr'')_5$"; however, the uniformity of the film does not correlate with quality of the ferroelectric properties: "$Nb(OAr'')_5$" < $Nb(OEt)_5$ < **1** < **3**. It appears that the reduction, but not complete elimination, of hydrolyzable ligands is desirable. The properties of the films generated using **1** and **3** indicates that the THME and ONp ligands control the hydrolysis and yield improved microstructures versus $Nb(OEt)_5$. The reduction of hydrolysis using ONp ligands has been previously noted for the $[Ti(ONp)_4]_2$ system.[92] Using these complexes superior ferroelectric properties of the resultant PNZT films where observed versus the "$Nb(OAr'')_5$" or $Nb(OEt)_5$ doped materials.

Conclusion

Three novel Nb alkoxide complexes have been synthesized and completely characterized: $[Nb(\mu\text{-}OEt)(ONp)_4]_2$, $[(\mu\text{-}BHMP)Nb_2(\mu\text{-}O)(OEt)_5]_2$, and $[(\mu\text{-}THME)Nb(OEt)_2]_2$. Upon alcoholysis exchange, $Nb(OEt)_5$, a dinuclear complex in solution, exchanges only terminal ligands. The BHMP ligand acts as tetradentate ligand-forming molecular voids, the size of which are dictated by the BHMP ligand. The THME ligand forms a dinuclear complex with the THME ligand acting as both a chelating and bridging ligand.

Solution ^{93}Nb NMR has been useful for identifying the multinuclear equilibrium of these compounds that are not easily interpreted or observed using standard nuclei. One explanation of this phenomenon is that we are seeing only exchange-averaged ^1H and ^{13}C resonances, wherein in the ^{93}Nb spectrum individual non-average species are observed due to a much larger spectral dispersion. The range of shifts observed for the various $Nb(OR)_5$ is relatively small but based on previous work, the structural characterization of **1**−**3**, and the ^{93}Nb NMR spectroscopic studies performed, we feel a multinuclear equilibrium exists at room temperature and mononuclear complexes dominate at high temperatures.

Introduction of **1** and **3** into our novel methods for generation of PMN and PNZT thin films and powders were successfully accomplished. From the variety of precursors we have synthesized and utilized, it is apparent that the sterically hindered **1** and **3** precursors are preferred for materials application to existing $Nb(OEt)_5$ species. These compounds have reduced but not eliminated the number of hydrolyzable ligands that yields acceptable microstructures and high-quality PNZT ferroelectric films. Interestingly, the most uniform films do not necessarily generate the highest quality ferroelectric properties. Furthermore, on the basis of the ^{93}Nb NMR results it is apparent that solution temperature will influence the nuclearity of the precursors, and thus the properties of the final materials made using these compounds. Further work to understand microstructural influences and final film properties is underway.

Acknowledgment. This work supported by the United States Department of Energy under Contract DE-AC04-94AL85000. Sandia is a multiprogram laboratory operated by Sandia Corp., a Lockeed Martin company, for the United States Department of Energy. The authors would like to thank the following employees of Sandia National Laboratories: M. A. Rodriguez, M. Gonzales, and R. Tissot for XRD studies, W. Chambers for ICP results, G. Zender and B. McKenzie for SEM. Special thanks to Peter K. Dorhout (C.S.U.) for preliminary ESMS experiments and William E. Buhro (Washington University) for sharing information prior to publication.

Supporting Information Available: Complete set of crystal data including positional parameters, bond distances, angles, thermal parameters for **1**−**3** (31 pages); structure factor tables (19 pages). Ordering information is given on any current masthead page.

CM970506P

(90) Boyle, T. J.; Dimos, D. B.; Alam, T. M.; Schwartz, R. W.; Buchheit, C. D.; Sinclair, M. B. *J. Mater. Res.* **1997**, *12*, 1022.

(91) Personal communication with M. A. Rodriquez, X-ray Laboratory of Sandia National Laboratories.

(92) Boyle, T. J.; Alam, T. M.; Mechenbeir, E. J.; Scott, B.; Ziller, J. W. *Inorg. Chem.* **1997**, *36*, 3293.